Comparison between local elasticity and non-local peridynamics

Olaf Weckner*, Gerd Brunk,
Michael A. Epton, Stewart A. Silling, Ebrahim Askari

February 13, 2009

Abstract

In this paper we compare small deformations in an infinite linear elastic body due to the presence of point loads within the classical, local formulation to the corresponding deformations in the peridynamic, non-local formulation. Due to the linearity of the problem the response to a point load can then be used to obtain the response to general loading functions by superposition. Using LAPLACE and FOURIER transforms we first derive an integral representation for the 3D peridynamic solution with the help of GREEN's functions. Dynamic and static examples in 1D and 3D using this theoretical result illustrate interesting differences between the local and non-local formulation. Explicit analytical solutions are obtained where possible. Numerical methods are used when needed and also for verification.

1 Introduction

The prediction of the spontaneous nucleation of cracks as well as the subsequent propagation in load-carrying structures such as the wing of an airplane presents a long-standing problem in continuum mechanics of solids. In a complex loading situation such as a bird strike multiple interacting cracks can be present at the same time. The generally curvilinear path along which a crack propagates in a three dimensional structure is not known a priori and must be determined as part of the solution. In addition the crack path also depends on the *material*. Recently anisotropic composite materials (such as CFRP) are replacing more traditional isotropic materials (such as aluminum) in part because of their higher specific strength, promising significant weight savings. For a given loading the crack path in a composite structure depends on the details of the underlying microstructure.
The level of fidelity of simulations using traditional FE codes in predicting inelastic material behavior has lagged behind their capabilities in elastic stress analysis. This difficulty

*Corresponding author. Olaf Weckner, Applied Math. The Boeing Company. P.O. Box 3707 MS 7L-25, Seattle, WA 98124, USA. Tel.: +1 425 373 2741. olaf@weckner.de

arises in part because the mathematical framework on which these methods are based assumes that the body remains continuous as it deforms. Hence, these methods break down at a crack tip and special techniques must be used which typically require the path of the crack to be known in advance, amongst other difficulties.
As an attempt at improving this situation, a theory of continuum mechanics known as peridynamics has been recently proposed by Silling [36]. Silling realized that the aforementioned limitations cannot be removed by further attempts to retrofit the traditional FE methods. The objective of peridynamics is to reformulate the basic mathematical description in such a way that the same equations hold both at a crack tip as well as in the far field. In this approach internal forces are expressed through pairwise interactions, so-called bonds, between pairs of material points. The finite interaction distance introduces non-locality. The complete constitutive model, including damage, is determined at the bond level. Cracks grow when and where it is energetically favorable for them to do so.
Non-local theories in continuum mechanics have been known since the 1970s from articles by Kröner [23], Eringen [17, 18], Edelen [19], Kunin [24], Rogula [33] and co-authors. These theories aim to describe certain effects which are not captured accurately in the corresponding local formulation, e.g. the physically unreasonable infinite stresses found at a crack tip in local linear elasticity. More recently, non-local approaches have been discussed e.g. in [5, 6, 8, 31, 32, 36, 43, 44, 11, 26]. Among these approaches peridynamics falls into the category of strongly non-local methods. Recent theoretical developments in peridynamics can be found in [15, 47, 10, 40, 25, 39, 45, 16, 46]. In [1, 3, 7, 9, 12, 20, 21, 49, 30, 27, 29, 34, 37, 38, 48] simulations based primarily on an numerical implementation of peridynamics called EMU [35] cover a wide range of very interesting problems involving the spontaneous initiation of discontinuities followed by their unguided propagation.
However, the study of strictly elastic problems and their relationship to the classical local formulation has been somewhat neglected. This neglect stems from the following. Local elasticity is well understood and yields satisfactory results for a large class of important problems typically involving the determination of the stress and strain fields. While it is possible to solve the same set of elastic problems using the non-local peridynamic formulation, the computational costs would be considerably higher. However, the fidelity of the classical approach in determining the initiation and propagation of cracks is clearly lagging behind its ability to determine elastic stress and strain fields. Peridynamics has been developed in an effort to close this gap in predicting *inelastic* deformations.
However, in order to increase the fidelity in predicting *inelastic* material behavior a full understanding of the *elastic* case is essential which is the focus of this paper.

The paper is organized as follows. In section 2 previous research using Green's functions for elastic problems in 1D is summarized and in section 3 this approach is extended to the 3D case. This section also contains a careful comparison between local and non-local elasticity, including a previously unpublished formulation for the 3D FE discretization of the peridynamic equation of motion. Examples are given in section 4. Section 5 concludes and discusses open questions.

2 Local and non-local elastic deformations in 1D

The equation of motion at time t for the material point x in an infinite, homogeneous body in one spatial dimension is

$$\rho\,\ddot{u}(x,t) \;=\; \mathcal{L}[u(x,t)] + b(x,t) \tag{1}$$

where the linear operator $\mathcal{L}$ acting on the displacement field $u(x,t)$ captures internal forces while $b(x,t)$ captures external forces. ρ is the density.[1]
In local elasticity the internal forces are represented by the differential operator

$${}^{L}\mathcal{L}[u(x,t)] \;=\; E\frac{\partial^2 u(x,t)}{\partial^2 x} \tag{2}$$

with YOUNG's modulus E. This is the well-known wave equation. On the other hand, the non-local peridynamic formulation for an infinite linear micro-elastic material leads to the integral operator

$${}^{NL}\mathcal{L}[u(x,t)] \;=\; \int_{-\infty}^{+\infty} c(x'-x)[\,u(x',t)-u(x,t)\,]dx' \tag{3}$$

with the so-called micromodulus function $c(\xi) = c(-\xi)$.
The associated energy balance is obtained by multiplying the equation of motion (1) by the velocity and subsequent integration over the body[2]:

$$\begin{aligned}
\dot{E}_{tot}(t) &= P(t) \qquad (4)\\
P(t) &= \int_{-\infty}^{+\infty} b(x,t)\dot{u}(x,t)dx\\
E_{tot}(t) &= E_{kin}(t) + E_{el}(t)\\
E_{kin}(t) &= \int_{-\infty}^{+\infty} \frac{\rho}{2}\left(\dot{u}(x,t)\right)^2 dx\\
{}^{L}E_{el}(t) &= \int_{-\infty}^{+\infty} \frac{1}{2}\left(\frac{\partial u(x,t)}{\partial x}\right)^2 dx\\
{}^{NL}E_{el}(t) &= \int_{-\infty}^{+\infty}\int_{-\infty}^{+\infty} \frac{c(x'-x)}{4}(u(x',t)-u(x,t))^2 dx'dx
\end{aligned}$$

[1] Equation (1) has the same form for both local and non-local formulation. However, the operator $\mathcal{L}$ is different and so is the solution. This will be indicated by the superscripts ${}^{L}(\cdot)$, ${}^{NL}(\cdot)$ in the following.

[2] This can be verified by taking the time derivative inside the integral and substituting the corresponding equation of motion.

Given the initial data $u_0(x) = u(x, t = 0), v_0(x) = \dot{u}(x, t = 0)$ it has been shown in [46] that the solution of (1) has the following integral representation

$$
\begin{aligned}
u(x,t) &= \int_{-\infty}^{+\infty} u_0(x-\hat{x})\dot{g}(\hat{x},t)d\hat{x} + \int_{-\infty}^{+\infty} v_0(x-\hat{x})g(\hat{x},t)d\hat{x} \qquad (5)\\
&\quad + \int_0^t \int_{-\infty}^{+\infty} \frac{b(x-\hat{x},t-\hat{t})}{\rho} g(\hat{x},\hat{t})d\hat{x}d\hat{t} \quad \text{where}\\
g(x,t) &= \mathcal{F}_{1D}^{-1}\{\frac{\sin(\omega(k)t)}{\omega(k)}\} \equiv \frac{1}{2\pi}\int_{-\infty}^{+\infty} e^{ikx}\frac{\sin((\omega(k)t)}{\omega(k)}dk \quad \text{and}\\
{}^{L}\omega(k) &= c_0\, k \text{ with the speed of sound, } c_0 = \sqrt{E/\rho}\\
{}^{NL}\omega(k) &= \left(\int_{-\infty}^{+\infty}(1-\cos(k\xi))c(\xi)d\xi/\rho\right)^{1/2}
\end{aligned}
$$

3 Local and non-local elastic deformations in 3D

3.1 Kinematics

The material particles X are addressed by their position in the reference configuration at say $t = 0$, represented by their position vectors $\boldsymbol{x} \in \mathbb{R}^3$. At time t the particle X has moved to its current position $\boldsymbol{y}(\boldsymbol{x}, t) = \boldsymbol{x} + \boldsymbol{u}(\boldsymbol{x}, t)$ where $\boldsymbol{u}$ is the displacement field. The velocity of particle X is defined as $\boldsymbol{v}(\boldsymbol{x}, t) = \dot{\boldsymbol{y}}(\boldsymbol{x}, t) = \dot{\boldsymbol{u}}(\boldsymbol{x}, t)$. The relative position of two particles X and X' in the reference configuration is denoted by $\boldsymbol{\xi} = \boldsymbol{x}' - \boldsymbol{x}$ and is called a peridynamic bond. The corresponding relative position in the current configuration is given by $\boldsymbol{y}(\boldsymbol{x}', t) - \boldsymbol{y}(\boldsymbol{x}, t) = \boldsymbol{\xi} + \boldsymbol{\eta} = (\xi + \eta)\boldsymbol{n}_{\boldsymbol{\xi}+\boldsymbol{\eta}}$ with the relative displacement $\boldsymbol{\eta} = \boldsymbol{u}(\boldsymbol{x}', t) - \boldsymbol{u}(\boldsymbol{x}, t)$ and the unit vector pointing from particle X towards particle X', $\boldsymbol{n}_{\boldsymbol{\xi}+\boldsymbol{\eta}}$. For smooth deformation fields we can introduce the deformation gradient $\boldsymbol{F}(\boldsymbol{x}, t) = (\nabla \boldsymbol{y}(\boldsymbol{x}, t))^T$: $\boldsymbol{\xi} + \boldsymbol{\eta} = \boldsymbol{F} \cdot \boldsymbol{\xi} + O(\xi^2)$ or $d\boldsymbol{y}(\boldsymbol{x}, t)|_t = \boldsymbol{F}(\boldsymbol{x}, t) \cdot d\boldsymbol{x}$. Due to the balance of linear and angular momentum the non-local force that particle X' exerts on X must be a central force, $\boldsymbol{f}(\boldsymbol{x}, \boldsymbol{x}', t) = f(\boldsymbol{x}, \boldsymbol{x}', t)\boldsymbol{n}_{\boldsymbol{\xi}+\boldsymbol{\eta}}$. These quantities are illustrated in the following graphic.

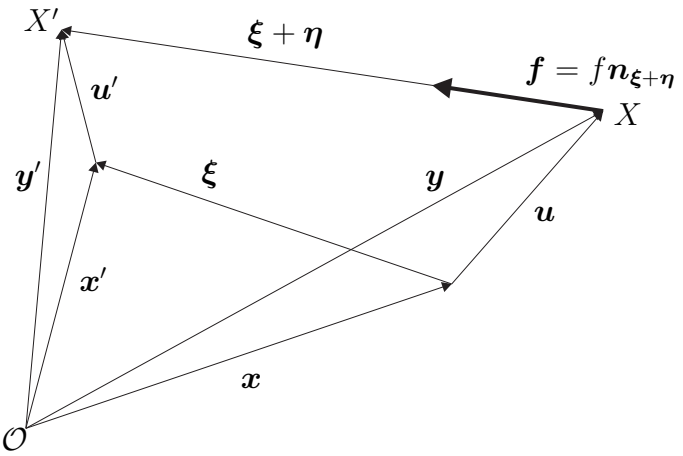

Fig. 1: Kinematics

3.2 Comparison of local and non-local elasticity

3.2.1 Equation of motion

The equation of motion at time $t \in \mathcal{T} = (0, T)$ for the material point $\boldsymbol{x} \in \mathcal{B}$ in an infinite, linear elastic, isotropic, homogeneous body $\mathcal{B} = \mathbb{R}^3$ as formulated within the framework of local continuum mechanics is given by the the NAVIER equations, see e.g. [14]:

$$\begin{aligned} \rho\, \ddot{\boldsymbol{u}}(\boldsymbol{x},t) &= \nabla \cdot \boldsymbol{S}(\boldsymbol{x},t) + \boldsymbol{b}(\boldsymbol{x},t) \\ \boldsymbol{S}(\boldsymbol{x},t) &= 2\mu\, \boldsymbol{\varepsilon}(\boldsymbol{x},t) + \lambda\, \mathrm{Tr}(\boldsymbol{\varepsilon}(\boldsymbol{x},t))\boldsymbol{I} \\ \boldsymbol{\varepsilon}(\boldsymbol{x},t) &= \frac{1}{2}\left(\nabla \boldsymbol{u}(\boldsymbol{x},t) + (\nabla \boldsymbol{u}(\boldsymbol{x},t))^T\right) \end{aligned} \tag{6}$$

with the reference density ρ, the 2nd PIOLA-KIRCHHOFF stress tensor $\boldsymbol{S}$, CAUCHY's infinitesimal strain tensor $\boldsymbol{\varepsilon}$ and the external force field $\boldsymbol{b}$. λ and μ are the LAMÉ constants which can alternatively be expressed in terms of the YOUNG's modulus $E = \mu\frac{3\lambda+2\mu}{\lambda+\mu}$ and the POISSON ratio $\nu = \frac{\lambda}{2(\lambda+\mu)}$. At time $t = 0$ we have the initial conditions

$$\begin{aligned} \boldsymbol{u}^0(\boldsymbol{x}) &= \boldsymbol{u}(\boldsymbol{x},0) \\ \boldsymbol{v}^0(\boldsymbol{x}) &= \dot{\boldsymbol{u}}(\boldsymbol{x},0) \end{aligned} \tag{7}$$

In the strongly non-local peridynamic formulation of continuum mechanics, see [36], the equation of motion for an infinite, isotropic, homogeneous, linear microelastic, pairwise equilibrated material takes the form

$$\rho\, \ddot{\boldsymbol{u}}(\boldsymbol{x},t) = \int_{\mathcal{H}(\boldsymbol{x},\delta)} \boldsymbol{C}(\boldsymbol{\xi}) \cdot [\boldsymbol{u}(\boldsymbol{x}+\boldsymbol{\xi},t) - \boldsymbol{u}(\boldsymbol{x},t)]\, dV_\xi + \boldsymbol{b}(\boldsymbol{x},t) \tag{8}$$

$$\boldsymbol{C}(\boldsymbol{\xi}) = \Lambda(\xi)\boldsymbol{\xi}\boldsymbol{\xi} \tag{9}$$

where the interaction "horizon" $\mathcal{H}(\boldsymbol{x}, \delta)$ is taken to be the sphere with center $\boldsymbol{x}$ and radius $\delta \in (0, \infty]$. The symmetric micromodulus tensor $\boldsymbol{C}(\boldsymbol{\xi}) = \boldsymbol{C}(-\boldsymbol{\xi}) = \boldsymbol{C}^T(\boldsymbol{\xi})$, more precisely, the micromodulus function $\Lambda(\xi)$, contains all constitutive information.
Formally, the differential operator of local elasticity has been replaced by the non-local peridynamic integral operator:

$$\rho\, \ddot{\boldsymbol{u}}(\boldsymbol{x}, t) = \mathcal{L}[\boldsymbol{u}(\boldsymbol{x}, t)] + \boldsymbol{b}(\boldsymbol{x}, t) \tag{10}$$

$$^{L}\mathcal{L}[\boldsymbol{u}(\boldsymbol{x}, t)] = (\lambda + \mu)\, \boldsymbol{\nabla}\boldsymbol{\nabla} \cdot \mathbf{u}(\mathbf{x}, \mathbf{t}) + \mu\, \boldsymbol{\nabla} \cdot \boldsymbol{\nabla}\mathbf{u}(\mathbf{x}, \mathbf{t}) \tag{11}$$

$$^{NL}\mathcal{L}[\boldsymbol{u}(\boldsymbol{x}, t)] = \int_{\mathcal{H}(\boldsymbol{x}, \delta)} \boldsymbol{C}(\boldsymbol{\xi}) \cdot [\boldsymbol{u}(\boldsymbol{x} + \boldsymbol{\xi}, t) - \boldsymbol{u}(\boldsymbol{x}, t)]\, dV_{\xi} \tag{12}$$

3.2.2 Jump conditions

One first important difference between the local and non-local formulation is the jump condition for linear momentum formulated across a moving discontinuity surface $\mathcal{A}(t)$. The spatial (immaterial) point $\boldsymbol{y}_{\mathcal{A}}(t) \in \mathcal{A}(t)$ momentarily occupies the material point $\boldsymbol{x}_{\mathcal{A}}(t)$, so $\boldsymbol{y}_{\mathcal{A}}(t) = \boldsymbol{y}(\boldsymbol{x}_{\mathcal{A}}(t), t)$. At $\boldsymbol{y}_{\mathcal{A}}$, $\mathcal{A}(t)$ has the surface normal $\boldsymbol{n}_{\mathcal{A}}(t)$ and velocity[3] $\boldsymbol{v}_{\mathcal{A}}(t) = \boldsymbol{F}^{+} \cdot \dot{\boldsymbol{x}}_{\mathcal{A}} + \boldsymbol{v}^{+} = \boldsymbol{F}^{-} \cdot \dot{\boldsymbol{x}}_{\mathcal{A}} + \boldsymbol{v}^{-}$. At the fixed time t the linear momentum jump condition reads as[4]

$$\boldsymbol{n}_{\mathcal{A}} \cdot [[(\boldsymbol{v} - \boldsymbol{v}_{\mathcal{A}})\, \tilde{\rho}\, \boldsymbol{v}]] = \begin{cases} \boldsymbol{n}_{\mathcal{A}} \cdot [[\boldsymbol{S}]] & \text{Local} \\ \mathbf{0} & \text{Non-local} \end{cases} \tag{13}$$

where $\tilde{\rho}$ is the mass per unit volume in the actual configuration which is related to the reference density by $\rho = \det(\boldsymbol{F})\, \tilde{\rho}$. The jump conditions for mass and continuity of displacement are identical in both formulations:

$$\boldsymbol{n}_{\mathcal{A}} \cdot [[(\boldsymbol{v} - \boldsymbol{v}_{\mathcal{A}})\, \tilde{\rho}]] = 0 \quad \text{Balance of mass} \tag{14}$$

$$[[\boldsymbol{F}]] \cdot \dot{\boldsymbol{x}}_{\mathcal{A}} + [[\boldsymbol{v}]] = \mathbf{0} \quad \text{Continuity} \tag{15}$$

Substituting equation (14) into the non-local equation (13) and assuming that the deformation is such that the density always remains positive ($\det(\boldsymbol{F}) > 0$) it follows that

$$\boldsymbol{n}_{\mathcal{A}} \cdot \left(\boldsymbol{v}^{+} - \boldsymbol{v}_{\mathcal{A}}\right) [[\boldsymbol{v}]] = 0 \tag{16}$$

If we choose an arbitrary, immaterial discontinuity surface with $\boldsymbol{n}_{\mathcal{A}} \cdot \boldsymbol{v}^{+} \neq \boldsymbol{n}_{\mathcal{A}} \cdot \boldsymbol{v}_{\mathcal{A}}$, it follows from equation (16) that we cannot have a jump in the velocity field. In a continuous deformation equation (15) then implies that the deformation gradient tensor, and therefore the strain tensor, must be continuous as well. This is the trivial case where all the fields are smooth.
On the other hand, if we assume an (initial) velocity field with a jump discontinuity as in the

[3] Here $\boldsymbol{\phi}^{+}$ and $\boldsymbol{\phi}^{-}$ are the values of $\boldsymbol{\phi}$ from positive and negative sides of $\boldsymbol{n}_{\mathcal{A}}$ of $\mathcal{A}$ and $[[\boldsymbol{\phi}]] := \boldsymbol{\phi}^{+} - \boldsymbol{\phi}^{-}$.
[4] See e.g. [42] for a derivation.

case of the well-known RIEMANN problem, eqs (16, 14) imply $\boldsymbol{n}_{\mathcal{A}}\cdot\boldsymbol{v}^{+} = \boldsymbol{n}_{\mathcal{A}}\cdot\boldsymbol{v}^{-} = \boldsymbol{n}_{\mathcal{A}}\cdot\boldsymbol{v}_{\mathcal{A}}$ or $\boldsymbol{v}_{\mathcal{A}} = \boldsymbol{v}^{+}\cdot\boldsymbol{n}_{\mathcal{A}}\,\boldsymbol{n}_{\mathcal{A}} + \boldsymbol{v}^{\perp}_{\mathcal{A}}$ with $\boldsymbol{v}^{\perp}_{\mathcal{A}}\cdot\boldsymbol{n}_{\mathcal{A}} = 0$. This means that in a non-local deformation which respects both balance of mass and linear momentum the normal component of the velocity field is always continuous and any discontinuity surface moves like a material interface in the normal direction. The only possible velocity jumps lie in the tangent plane that locally coincides with the generally curved discontinuity surface: $[[\boldsymbol{v}\cdot\boldsymbol{P}_{\boldsymbol{n}_{\mathcal{A}}}]] \neq \boldsymbol{0}$ with the projector $\boldsymbol{P}_{\boldsymbol{n}_{\mathcal{A}}} = \boldsymbol{I} - \boldsymbol{n}_{\mathcal{A}}\boldsymbol{n}_{\mathcal{A}}$. Since $\boldsymbol{v}_{\mathcal{A}}(t) = \boldsymbol{F}^{+}\cdot\dot{\boldsymbol{x}}_{\mathcal{A}} + \boldsymbol{v}^{+}$ it follows that $\boldsymbol{n}_{\mathcal{A}}\cdot\boldsymbol{F}^{+}\cdot\dot{\boldsymbol{x}}_{\mathcal{A}} = 0$. For arbitrary $\boldsymbol{n}_{\mathcal{A}}$ and $\det(\boldsymbol{F}^{+}) > 0$ this implies $\dot{\boldsymbol{x}}_{\mathcal{A}} = \boldsymbol{0}$. However, according to equation (15) this is no longer compatible with a discontinuous velocity field.
In summary, a jump in the velocity field can only occur in the components that lie in the plane tangent to the discontinuity surface $\mathcal{A}$. It is always accompanied by a jump in displacement field, the location of which is fixed at the LAGRANGian point $\boldsymbol{x}_{\mathcal{A}}$[5]. This is an important difference between the non-local and local formulation, the latter allowing for shock-waves in which both velocity and strain field can simultaneously be discontinuous.

3.2.3 Energy balance

The energy balance associated with the equation of motion (10) is obtained by multiplication with the velocity field $\boldsymbol{v}(\boldsymbol{x},t)$ and integration over the domain $\mathcal{B}$:

$$
\begin{aligned}
\dot{E}_{tot}(t) &= P(t) \qquad (17)\\
P(t) &= \int_{\mathcal{B}} \boldsymbol{b}(\boldsymbol{x},t)\cdot\boldsymbol{v}(\boldsymbol{x},t)dV_x\\
E_{tot} &= E_{kin}(t) + E_{el}(t)\\
E_{kin,\,el}(t) &= \int_{\mathcal{B}} e_{kin,\,el}(\boldsymbol{x},t)dV_x\\
e_{kin}(\boldsymbol{x},t) &= \frac{\rho}{2}\boldsymbol{v}(\boldsymbol{x},t)^2\\
{}^{L}e_{el}(\boldsymbol{x},t) &= \frac{1}{2}\boldsymbol{S}(\boldsymbol{x},t)\cdot\cdot\,\boldsymbol{\varepsilon}(\boldsymbol{x},t)\\
{}^{NL}e_{el}(\boldsymbol{x},t) &= \frac{1}{2}\int_{\mathcal{H}(\boldsymbol{x},\delta)} w(\boldsymbol{\xi},\boldsymbol{u}(\boldsymbol{x}+\boldsymbol{\xi},t)-\boldsymbol{u}(\boldsymbol{x},t))dV_\xi\\
w(\boldsymbol{\xi},\boldsymbol{\eta}) &= \frac{1}{2}\boldsymbol{\eta}\cdot\boldsymbol{C}(\boldsymbol{\xi})\cdot\boldsymbol{\eta}
\end{aligned}
$$

The definition of the kinetic energy and the power of the external forces is the same in both local and non-local elasticity while the elastic energy differs: the non-local elastic energy density is given by the integration of the pairwise potential $w(\boldsymbol{\xi},\boldsymbol{\eta}) : \partial_{\boldsymbol{\eta}} w(\boldsymbol{\xi},\boldsymbol{\eta}) = \boldsymbol{C}(\boldsymbol{\xi})\cdot\boldsymbol{\eta} = \boldsymbol{f}(\boldsymbol{x},\boldsymbol{x}',t)$ over the horizon. For example, in a homogeneous deformation characterized by a constant deformation gradient $\boldsymbol{F}_0$ we have ${}^{L}e_{el} = \frac{\lambda+2\mu}{2}I_1^2 - 2\mu\,I_2$ and ${}^{NL}e_{el} = \frac{\pi}{15}\int_0^\delta \xi^6\Lambda(\xi)d\xi\,[\,3I_1^2 - 4I_2\,]$ with the first and second invariants of the strain tensor $\boldsymbol{\varepsilon}_0 = \frac{1}{2}(\boldsymbol{F}_0^T\cdot\boldsymbol{F}_0 - \boldsymbol{I})$: $I_1 = \mathrm{Tr}(\boldsymbol{\varepsilon}) = \varepsilon_I + \varepsilon_{II} + \varepsilon_{III}$ and $I_2 = \varepsilon_I\varepsilon_{II} + \varepsilon_{II}\varepsilon_{III} + \varepsilon_{III}\varepsilon_I$, see [2].

[5] In [46] analogous results were obtained for the 1D case.

Requiring that the elastic energy density for any homogeneous deformation is identical in both local and non-local elasticity leads to the restriction[6]

$$\lambda \;=\; \mu \quad \text{or} \quad \nu = \frac{1}{4} \tag{18}$$

It further relates the micromodulus function Λ to the LAMÉ constant λ

$$\int_0^\delta \Lambda(r) r^6 dr \;=\; \frac{15\lambda}{2\pi} \tag{19}$$

3.2.4 Equation of motion in FOURIER space

Applying the FOURIER-transform with respect to the spatial coordinate $\boldsymbol{x}$ we can equivalently characterize the equation of motion (10) by the acoustic tensor $\boldsymbol{M}(\boldsymbol{k})$ as follows[7]

$$\begin{aligned}
\rho\, \ddot{\bar{\boldsymbol{u}}}(\boldsymbol{k},t) \;+\; & \boldsymbol{M}(\boldsymbol{k}) \cdot \bar{\boldsymbol{u}}(\boldsymbol{k},t) = \bar{\boldsymbol{b}}(\boldsymbol{k},t) && (20)\\
\boldsymbol{M}(\boldsymbol{k}) \;=\; & M_\parallel(k) \boldsymbol{n_k} \boldsymbol{n_k} + M_\perp(k) \boldsymbol{P}_{\boldsymbol{n_k}} && (21)\\
{}^{L}M_\parallel(k) \;=\; & (\lambda + 2\mu)\; k^2 && (22)\\
{}^{L}M_\perp(k) \;=\; & \mu\; k^2 && (23)\\
{}^{NL}M_\parallel(k) \;=\; & 4\pi \int_0^\delta \Lambda(r) r^4 A_1(kr) dr && (24)\\
{}^{NL}M_\perp(k) \;=\; & 4\pi \int_0^\delta \Lambda(r) r^4 A_2(kr) dr && (25)\\
A_1(x) \;=\; & \frac{1}{3} - \frac{\sin(x)}{x} - \frac{2\cos(x)}{x^2} + \frac{2\sin(x)}{x^3} && (26)\\
\;=\; & \sum_{k=0}^{\infty} \frac{(-1)^k x^{2k+2}}{(2k+2)!(2k+5)} = \frac{x^2}{10} + O(x^4) \\
A_2(x) \;=\; & \frac{1}{3} + \frac{\cos(x)}{x^2} - \frac{\sin(x)}{x^3} && (27)\\
\;=\; & \sum_{k=0}^{\infty} \frac{(-1)^k x^{2k+2}}{(2k+3)!(2k+5)} = \frac{x^2}{30} + O(x^4)
\end{aligned}$$

The transformed initial conditions are

$$\begin{aligned}
\bar{\boldsymbol{u}}^0(\boldsymbol{k}) \;=\; & \mathcal{F}\{\boldsymbol{u}^0(\boldsymbol{x})\} && (28)\\
\bar{\boldsymbol{v}}^0(\boldsymbol{k}) \;=\; & \mathcal{F}\{\boldsymbol{v}^0(\boldsymbol{x})\}
\end{aligned}$$

[6]This restriction is only present in the bond-based formulation and no longer present in the so-called state-based peridynamic formulation, see [39].

[7]The local case can be obtained by using the formula for the FOURIER-transforms of derivatives given in section 7.2.2. In the non-local case one first uses the convolution theorem given in section 7.2.3 to obtain the acoustic tensor ${}^{NL}\boldsymbol{M}(\boldsymbol{k}) = \bar{\boldsymbol{C}}(\boldsymbol{0}) - \bar{\boldsymbol{C}}(\boldsymbol{k})$. Carrying out the required integration for the inverse FOURIER-transform in spherical coordinates and using the result that $\int_{\mathcal{S}} e^{-i\boldsymbol{k}\cdot\boldsymbol{\xi}} \boldsymbol{n_\xi} \boldsymbol{n_\xi} dA_\xi / 4\pi = \frac{\sin(kx) - kx\cos(kx)}{(kx)^3} \boldsymbol{n_k} \boldsymbol{n_k} + \frac{((kx)^2 - 2)\sin(kx) + 2kx\cos(kx)}{(xk)^3} \boldsymbol{P}_{\boldsymbol{n_k}}$ where $\mathcal{S}$ is the unit sphere we obtain (20).

Using equation (19) together with eqs (26, 27) we see that the first non-zero term in the TAYLOR expansion of the the non-local acoustic tensor ${}^{NL}\boldsymbol{M}(\boldsymbol{k})$ in the large wavelength limit $k \to 0$ coincides with the local acoustic tensor ${}^{L}\boldsymbol{M}(\boldsymbol{k})$ for materials with $\lambda = \mu$. Alternatively, the convergence of the non-local peridynamic equation (8) towards the local NAVIER equations (6) can be shown directly in $(\boldsymbol{x}, t)$-space, see [16] (linear bond-based formulation) and [40] (non-linear state-based formulation).

3.2.5 Wave propagation

A physical interpretation of the acoustic tensor can be obtained by studying the propagation of plane waves $\boldsymbol{u}(\boldsymbol{x}, t) = \hat{\boldsymbol{u}}\, e^{\imath\,(\boldsymbol{k}\cdot\boldsymbol{x} \pm \omega(k)\,t)}$ where $\omega(k)$ is the dispersion relation relating the angular frequency ω to the wave number $k = ||\boldsymbol{k}||$. Substituting the wave ansatz into the equation of motion (10) leads to the eigenvalue problem $\boldsymbol{M}(\boldsymbol{k}) \cdot \hat{\boldsymbol{u}} = \rho\,\omega(k)^2 \hat{\boldsymbol{u}}$. From this we can identify pressure and shear waves where $\hat{\boldsymbol{u}} = \hat{u}_{\parallel}\, \boldsymbol{n}_{\boldsymbol{k}}$ and $\hat{\boldsymbol{u}} = \hat{u}_{\perp}\, \boldsymbol{t}_k,\ \boldsymbol{t}_k \cdot \boldsymbol{n}_{\boldsymbol{k}} = 0$ traveling with the phase velocities

$$v_{\parallel}^{p}(k) = \frac{\omega_{\parallel}(k)}{k} \quad = \quad \sqrt{M_{\parallel}(k)/\rho k^2} \tag{29}$$

$$v_{\perp}^{p}(k) = \frac{\omega_{\perp}(k)}{k} \quad = \quad \sqrt{M_{\perp}(k)/\rho k^2} \tag{30}$$

In local elasticity the phase velocity does not depend on the wavelength for either pressure or shear waves: ${}^{L}v_{\parallel}^{p} = \sqrt{\lambda + 2\mu/\rho}$, ${}^{L}v_{\perp}^{p} = \sqrt{\mu/\rho}$, see eqs (22, 23). In contrast, peridynamics always leads to wave dispersion. Note that wave dispersion is present in most augmented models of continuum mechanics such as the weakly non-local higher order gradient theories, see e.g. [28] or the strongly non-local ERINGEN-type models, see e.g. [17]. These models aim to describe certain effects which are not captured accurately in local linear elasticity. One such example is the non-linearity found in experimentally measured dispersion relations, reflecting the inability of real materials to sustain waves of arbitrarily small wavelength as described in [22]. In this context it remains an important open question whether it is possible to determine the micromodulus function $\Lambda(\xi)$ from experimentally obtained dispersion data.
As an example, consider the case where all points interact: $\mathcal{H}(\boldsymbol{x}, \delta) = \mathbb{R}^3$. The micromodulus function is assumed to be either exponential $\Lambda_e(\xi) = \frac{\lambda}{\tilde{\delta}^7} \frac{8}{\pi^{3/2}} e^{-(\frac{\xi}{\tilde{\delta}})^2}$ or trigonometric $\Lambda_t(\xi) = \frac{\lambda}{\tilde{\delta}^7} \frac{15}{\pi^2} \frac{\sin\left(\frac{x}{\tilde{\delta}}\right) - \frac{x}{\tilde{\delta}} \cos\left(\frac{x}{\tilde{\delta}}\right)}{(\frac{x}{\tilde{\delta}})^7}$ where the length-scale $\tilde{\delta}$ determines the degree of non-locality. As shown below, the exponential form of the micromodulus function leads to wave dispersion for any finite wavelength $\chi = \frac{2\pi}{k}$ while the trigonometric micromodulus function behaves like a low-pass filter: waves with a wavelength larger than $\chi_c = 2\pi\delta$ travel with the same phase velocity as in the local formulation, waves smaller than the cut-off wavelength χ_c are dispersed. The exponential form of the micromodulus function results in the

following phase velocities as a function of the normalized wave number $\kappa = k\,\tilde{\delta}$

$$\frac{{}^{NL}v_{\parallel}^{p}(\kappa)}{\sqrt{\lambda/\rho}} = \sqrt{\frac{4+2e^{-\frac{\kappa^2}{4}}\,(\kappa^2-2)}{\kappa^2}} = \sqrt{3} - \frac{5}{16\sqrt{3}}\,\kappa^2 + O(\kappa^4) \tag{31}$$

$$\frac{{}^{NL}v_{\perp}^{p}(\kappa)}{\sqrt{\lambda/\rho}} = \sqrt{\frac{4-4e^{-\frac{\kappa^2}{4}}}{\kappa^2}} = 1 - \frac{1}{16}\,\kappa^2 + O(\kappa^4) \tag{32}$$

while the trigonometric micromodulus leads to

$$\frac{{}^{NL}v_{\parallel}^{p}(\kappa)}{\sqrt{\lambda/\rho}} = \begin{cases} \sqrt{3} & \kappa \leq 1 \\ \sqrt{\frac{5\kappa^3-2}{\kappa^5}} & \kappa > 1 \end{cases} \tag{33}$$

$$\frac{{}^{NL}v_{\perp}^{p}(\kappa)}{\sqrt{\lambda/\rho}} = \begin{cases} 1 & \kappa \leq 1 \\ \sqrt{\frac{5\kappa^3-5\kappa^2+1}{\kappa^5}} & \kappa > 1 \end{cases} \tag{34}$$

The large wavelengths expansion confirms the convergence towards local elasticity for materials with $\lambda = \mu$ as illustrated in the following graphic (left: exponential micromodulus, right: trigonometric micromodulus):

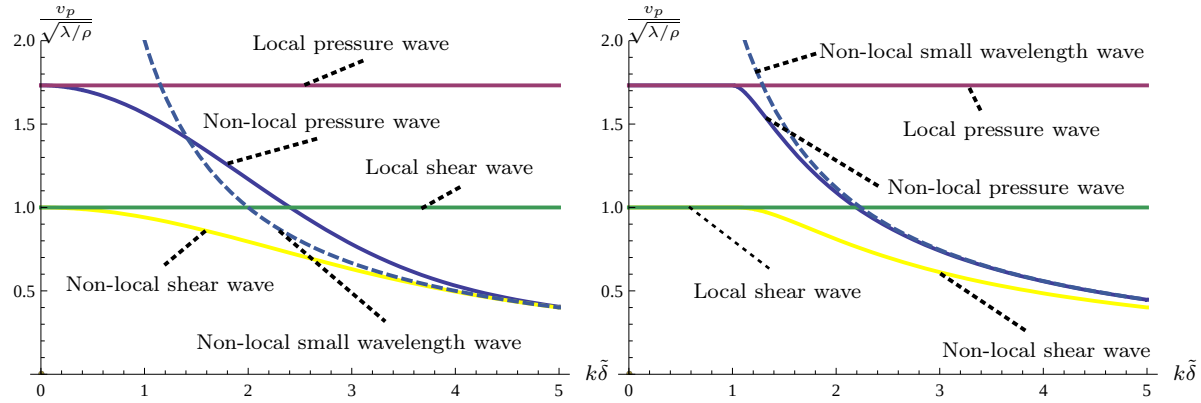

Fig. 2: Phase velocities in local and non-local elasticity

Furthermore, one can see that the components of the acoustic tensor become independent of the wave number in the small wavelength limit

$${}^{NL}M^{\infty} = {}^{NL}M_{\parallel}^{\infty} = {}^{NL}M_{\perp}^{\infty} = \frac{4\pi}{3}\int_0^{\delta} \Lambda(r) r^4 dr \tag{35}$$

so the phase velocity goes to zero as ${}^{NL}v^{p}(k) \sim \frac{\sqrt{{}^{NL}M^{\infty}/\rho}}{k}$. In the example above ${}^{NL}M_{e}^{\infty} = 4\lambda/\tilde{\delta}^2$ and ${}^{NL}M_{t}^{\infty} = 5\lambda/\tilde{\delta}^2$.

3.2.6 Weak formulation

Another way to characterize the motion $\boldsymbol{u}$ is given by the variational problem

$$\boldsymbol{u} \;=\; \operatorname{argmin} J[\boldsymbol{u}(\boldsymbol{x},t)], \quad J[\boldsymbol{u}(\boldsymbol{x},t)] = \int_{\mathcal{T}} \int_{\mathcal{B}} L(\boldsymbol{x},t) dV_x dt \tag{36}$$

where the Lagrangian density is given by $L(\boldsymbol{x},t) = e_{kin}(\boldsymbol{x},t) - e_{el}(\boldsymbol{x},t) - e_b(\boldsymbol{x},t)$ and the potential of the external force field is defined as $e_b(\boldsymbol{x},t) = -\boldsymbol{b}(\boldsymbol{x},t) \cdot \boldsymbol{u}(\boldsymbol{x},t)$. The EULER-LAGRANGE-equation associated with the variational problem (36) is the equation of motion (10), see [47]. The only difference between the local and the non-local formulation is again the elastic energy density.

3.2.7 Finite Element discretization

Finally one can also characterize the local and non-local formulations by their corresponding stiffness matrices. Introducing the RITZ-ansatz

$$\boldsymbol{u}_N(\boldsymbol{x},t) = \sum_{\alpha=1}^{N} \boldsymbol{u}^\alpha(t) g_\alpha(\boldsymbol{x}) \tag{37}$$

into the variational problem (36) leads to the discretized equation of motion for the $3N$ unknown displacements $u_i^\alpha(t) = \boldsymbol{e}_i \cdot \boldsymbol{u}^\alpha(t)$

$$\begin{gathered} \underset{\sim}{M}\, \underset{\sim}{\ddot{u}}\,(t) + \underset{\sim}{K}\, \underset{\sim}{u}\,(t) = \underset{\sim}{b}\,(t) \\ \Updownarrow \\ \sum_{j=1}^{3} \sum_{\beta=1}^{N} M_{\alpha,\beta}^{i,j} \ddot{u}_j^\beta(t) + \sum_{j=1}^{3} \sum_{\beta=1}^{N} K_{\alpha,\beta}^{i,j} u_j^\beta(t) = b_\alpha^i(t) \end{gathered} \tag{38}$$

The mass matrix and the inhomogeneity are identical in local and non-local elasticity

$$M_{\alpha,\beta}^{i,j} \;=\; \rho\, \delta^{ij} \int_{\mathcal{B}} g_\alpha(\boldsymbol{x}) g_\beta(\boldsymbol{x}) dV_x \tag{39}$$

$$b_\alpha^i(t) \;=\; \int_{\mathcal{B}} g_\alpha(\boldsymbol{x}) b^i(\boldsymbol{x},t) dV_x \quad \text{with} \quad b^i(\boldsymbol{x},t) = b_i(\boldsymbol{x},t) = \boldsymbol{e}_i \cdot \boldsymbol{b}(\boldsymbol{x},t) \tag{40}$$

while the local and non-local stiffness matrices differ

$${}^{L}K_{\alpha,\beta}^{ij} \;=\; \int_{\mathcal{B}} [\,(\lambda+\mu) \frac{\partial g_\alpha(\boldsymbol{x})}{\partial x_i} \frac{\partial g_\beta(\boldsymbol{x})}{\partial x_j} + \mu\, \delta^{ij} \sum_{k=1}^{3} \frac{\partial g_\alpha(\boldsymbol{x})}{\partial x_k} \frac{\partial g_\beta(\boldsymbol{x})}{\partial x_k}\,] dV_x \tag{41}$$

$${}^{NL}K_{\alpha,\beta}^{ij} \;=\; \int_{\mathcal{B}} \int_{\mathcal{B}} [g_\alpha(\boldsymbol{x}') - g_\alpha(\boldsymbol{x})] \frac{C^{ij}(\boldsymbol{x}'-\boldsymbol{x})}{2} [g_\beta(\boldsymbol{x}') - g_\beta(\boldsymbol{x})]\, dV_{x'} dV_x \quad \text{with} \tag{42}$$

$$C^{ij}(\boldsymbol{\xi}) \;=\; C_{ij}(\boldsymbol{\xi}) = \boldsymbol{e}_i \cdot \boldsymbol{C}(\boldsymbol{\xi}) \cdot \boldsymbol{e}_j = \Lambda(\xi) \xi_i \xi_j$$

where the limits of integration in the inner integral have been formally extended from $\mathcal{H}$ to the whole domain $\mathcal{B}$ since by definition $\boldsymbol{C}(\boldsymbol{\xi}) = \boldsymbol{0}\,\forall \xi \geq \delta$. The bandwidth of the stiffness matrix of local elasticity depends on the support of the basis function $g_\alpha(\boldsymbol{x})$. For computational efficiency one typically introduces a numerical length-scale δ_n such that $g_\alpha(\boldsymbol{x}) = 0\,\forall x \geq \delta_n$, $\forall \alpha$. Within the local formulation this leads to a sparse stiffness matrix with band structure. Within the non-local formulation the situation is more complex as there are two length-scales present, the numerical length-scale δ_n and the peridynamic horizon δ. To simplify the discussion we assume that $\delta = \infty$. Then the resulting non-local stiffness matrix will be dense, representing the physical interaction between any two particles in the body. Returning to the general case $\delta < \infty$ the non-local stiffness matrix will generally have a larger band-width than the local stiffness matrix. The higher computational costs are justified e.g. in the presence of propagating cracks (corresponding to discontinuous displacements) since this class of solutions are not contained in the SOBOLEV space associated with the weak formulation of the NAVIER equations.
Using the concept of DIRAC distributions $\Delta(x)$

$$\int_{\mathcal{I}} \delta^{(n)}(x-y) f(x) dx \;=\; (-1)^n f^{(n)}(y)\;\forall f(x) : y \in \mathcal{I},\; n \in \mathbb{N} \cup \{0\} \tag{43}$$

we recover the stiffness matrix of local elasticity for materials with $\lambda = \mu$ by formally setting[8]

$$\Lambda(\xi) = \frac{15\lambda}{2\pi} \frac{\Delta(\xi)}{\xi^6} \tag{44}$$

in equation (42). This demonstrates the convergence of the discretized non-local formulation towards the discretized local formulation.

3.3 Integral representation of the solution

Using the notation in appendix 7.3 we apply the LAPLACEtransformation with respect to time t to (20) and find the transformed solution $\tilde{\boldsymbol{u}}(\boldsymbol{k}, s) = \mathcal{L}\{\bar{\boldsymbol{u}}(\boldsymbol{k}, t)\}$:

$$\tilde{\boldsymbol{u}}(\boldsymbol{k}, s) \;=\; \big(\rho s^2 \boldsymbol{I} + \boldsymbol{M}(\boldsymbol{k})\big)^{-1} \cdot \Big(\tilde{\boldsymbol{b}}(\boldsymbol{k}, s) + s\,\bar{\boldsymbol{u}}^0(\boldsymbol{k}) + \bar{\boldsymbol{v}}^0(\boldsymbol{k})\Big) \tag{45}$$

$$\big(\rho s^2 \boldsymbol{I} + \boldsymbol{M}(\boldsymbol{k})\big)^{-1} \;=\; \frac{\boldsymbol{n_k} \boldsymbol{n_k}}{\rho s^2 + M_\parallel(k)} + \frac{\boldsymbol{P}_{\boldsymbol{n_k}}}{\rho s^2 + M_\perp(k)} \tag{46}$$

Knowing the individual LAPLACEtransforms

$$\mathcal{L}^{-1}\{\big(s^2 \boldsymbol{I} + \boldsymbol{T}(\boldsymbol{k})\big)^{-1}\} \;=\; \frac{\sin(\omega_\parallel(k)t)}{\omega_\parallel(k)} \boldsymbol{n_k} \boldsymbol{n_k} + \frac{\sin(\omega_\perp(k)t)}{\omega_\perp(k)} \boldsymbol{P}_{\boldsymbol{n_k}} =: \bar{\boldsymbol{g}}(\boldsymbol{k}, t) \tag{47}$$

$$\mathcal{L}^{-1}\{\tilde{\boldsymbol{b}}(\boldsymbol{k}, s) + s\,\bar{\boldsymbol{u}}^0(\boldsymbol{k}) + \bar{\boldsymbol{v}}^0(\boldsymbol{k})\} \;=\; \bar{\boldsymbol{b}}(\boldsymbol{k}, t) + \dot{\Delta}(t)\,\bar{\boldsymbol{u}}^0(\boldsymbol{k}) + \Delta(t)\,\bar{\boldsymbol{v}}^0(\boldsymbol{k}) \tag{48}$$

[8] Using the operator identity $x^n \delta^{(n)}(x) \equiv (-1)^n n! \Delta(x)\,\forall n \in \mathbb{N}$ we could alternatively set $\Lambda(\xi) = \frac{15\lambda}{2\pi} \frac{\Delta(\xi)''}{2\xi^4}$ or $\Lambda(\xi) = -\frac{15\lambda}{2\pi} \frac{\Delta(\xi)'}{\xi^5}$.

we can use the convolution theorem of LAPLACEtransforms to obtain the solution in FOURIER space:

$$\bar{\boldsymbol{u}}(\boldsymbol{k},t) \;=\; \int_{\mathcal{T}} \bar{\boldsymbol{g}}(\boldsymbol{k},t-\tau)\cdot\bar{\boldsymbol{b}}(\boldsymbol{k},\tau)d\tau + \dot{\bar{\boldsymbol{g}}}(\boldsymbol{k},t)\cdot\bar{\boldsymbol{u}}^0(\boldsymbol{k}) + \bar{\boldsymbol{g}}(\boldsymbol{k},t)\cdot\bar{\boldsymbol{v}}^0(\boldsymbol{k}) \tag{49}$$

Finally we use the convolution theorem of FOURIER-transforms to obtain the following integral representation of the solution of equation (10) in $(\boldsymbol{x},t)$ space

$$\begin{aligned}\boldsymbol{u}(\boldsymbol{x},t) \;=\; & \int_{\mathcal{B}} \boldsymbol{u}^0(\boldsymbol{x}-\hat{\boldsymbol{x}})\cdot\dot{\boldsymbol{g}}(\hat{\boldsymbol{x}},t)dV_{\hat{x}} \\ & + \int_{\mathcal{B}} \boldsymbol{v}^0(\boldsymbol{x}-\hat{\boldsymbol{x}})\cdot\boldsymbol{g}(\hat{\boldsymbol{x}},t)dV_{\hat{x}} \\ & + \int_{\mathcal{B}}\int_{\mathcal{T}} \frac{\boldsymbol{b}(\boldsymbol{x}-\hat{\boldsymbol{x}},t-\hat{t})}{\rho}\cdot\boldsymbol{g}(\hat{\boldsymbol{x}},\hat{t})d\hat{t}dV_{\hat{x}}\end{aligned} \tag{50}$$

with the GREEN's tensor[9]

$$\boldsymbol{g}(\boldsymbol{x},t) \;=\; \mathcal{F}^{-1}\{\bar{\boldsymbol{g}}(\boldsymbol{k},t)\} = \boldsymbol{n}_{\boldsymbol{x}}\boldsymbol{n}_{\boldsymbol{x}}\, g_{\boldsymbol{n}_{\boldsymbol{x}}}(x,t) + \boldsymbol{P}_{\boldsymbol{n}_{\boldsymbol{x}}}\, g_{\boldsymbol{P}_{\boldsymbol{n}_{\boldsymbol{x}}}}(x,t) \text{ with} \tag{51}$$

$$g_{\boldsymbol{n}_{\boldsymbol{x}}}(x,t) \;=\; \frac{1}{2\pi^2}\int_0^\infty k^2[\, a_1(xk)\left(\frac{\sin(\omega_\perp(k)t)}{\omega_\perp(k)} - \frac{\sin(\omega_\parallel(k)t)}{\omega_\parallel(k)}\right) + \frac{\sin(kx)}{kx}\frac{\sin(\omega_\perp(k)t)}{\omega_\perp(k)}\,]\,dk$$

$$g_{\boldsymbol{P}_{\boldsymbol{n}_{\boldsymbol{x}}}}(x,t) \;=\; \frac{1}{2\pi^2}\int_0^\infty k^2[\, a_2(xk)\left(\frac{\sin(\omega_\perp(k)t)}{\omega_\perp(k)} - \frac{\sin(\omega_\parallel(k)t)}{\omega_\parallel(k)}\right) + \frac{\sin(kx)}{kx}\frac{\sin(\omega_\perp(k)t)}{\omega_\perp(k)}\,]\,dk$$

where the notation $a_{1,2}(x) = A_{1,2}(x) - \frac{1}{3}$ has been used. Substituting (50, 51) into (10) confirms that the equation of motion is identically satisfied. Since $\boldsymbol{g}(\boldsymbol{x},0) = \boldsymbol{0}$ and $\dot{\boldsymbol{g}}(\boldsymbol{x},0) = \Delta(\boldsymbol{x})\boldsymbol{I}$ the initial conditions are satisfied as well.

4 Examples

In this chapter we consider the following examples:

- Transient dynamics of a bar (1D)
- Initial value problem for initial data with FOURIER-series representation (3D)
- Static solution for a single point load (3D)

[9] Applying an external force which is localized in both time and space, $\boldsymbol{b}(\boldsymbol{x},t) = \rho\,\Delta(t)\Delta(\boldsymbol{x})\boldsymbol{n}$, to a body initially at rest leads to the solution $\boldsymbol{u}(\boldsymbol{x},t) = \boldsymbol{n}\cdot\boldsymbol{g}(\boldsymbol{x},t)$.

4.1 Transient dynamics of a bar (1D)

In the following we consider a bar at rest for $t \leq 0$, subject to a pair of self-equilibrated point loads for $t > 0$:

$$\begin{aligned} u_0(x) &= 0 \\ v_0(x) &= 0 \\ b(x,t) &= \frac{F}{A}\left(\Delta(x-L) - \Delta(x+L)\right) \end{aligned} \tag{52}$$

This problem has been the topic of previous research. In [41] the *static* analytical solution for less smooth micromodulus functions $c \in C^D(\mathbb{R})$, $D < \infty$ is discussed. In [10] the *static* numerical solution is discussed in the context of adaptive grid refinement. In this paper we discuss the fully *dynamic* response, both numerically and analytically. We begin by introduce the normalization

$$\hat{x} = \frac{x}{L},\ \hat{t} = \frac{t}{L/c_0},\ \hat{u}(\hat{x},\hat{t}) = \frac{u(\hat{x}L, \hat{t}\frac{L}{c_0})}{2FL/EA},\ \hat{c}(\hat{x}) = \frac{c(\hat{x}L)}{E/L^3},\ \hat{b}(\hat{x},\hat{t}) = \frac{b(\hat{x}L, \hat{t}\frac{L}{c_0})}{2A/F},\ \hat{\omega}(\hat{k}) = \frac{\omega(\hat{k}/L)}{c_0/L}$$

where the displacement field has been normalized with the static elongation of a bar of length $2L$ subjected to a static force F in local elasticity. Then the solution for both local and non-local formulation is given by (5, 52)

$$\hat{u}(\hat{x},\hat{t}) = \frac{1}{2\pi}\int_{-\infty}^{+\infty} \frac{1-\cos(\hat{\omega}(\hat{k})\hat{t})}{\hat{\omega}^2(\hat{k})} \sin(\hat{k}\hat{x})\sin(\hat{k})d\hat{k} \tag{53}$$

From (53) we see that the displacements are antisymmetric, $\hat{u}(-\hat{x},\hat{t}) = -\hat{u}(\hat{x},\hat{t})$.

4.1.1 Classical local solution

Local elasticity corresponds to a linear dispersion relation, $\hat{\omega}(\hat{k}) = \hat{k}$. In this case we can evaluate equation (53) explicitly. The solution can be written as the superposition of the transient solution ${}^L_T\hat{u}(\hat{x},\hat{t})$ and the static solution ${}^L_S\hat{u}(\hat{x})$:

$${}^L\hat{u}(\hat{x},\hat{t}) = {}^L_T\hat{u}(\hat{x},\hat{t}) + {}^L_S\hat{u}(\hat{x}) \text{ with} \tag{54}$$

$$\begin{aligned} {}^L_T\hat{u}(\hat{x},\hat{t}) = 1/8\,[\ & (\mathrm{sgn}(1-\hat{x}+\hat{t}) + (\mathrm{sgn}(1-\hat{x}-\hat{t}) \\ & -(\mathrm{sgn}(1+\hat{x}+\hat{t}) - (\mathrm{sgn}(1+\hat{x}-\hat{t})\ ] \end{aligned} \tag{55}$$

$${}^L_S\hat{u}(\hat{x}) = \frac{1}{4}\left(|1+\hat{x}| - |1-\hat{x}|\right) \tag{56}$$

where $\mathrm{sgn}(x) = x/|x|$ is the sign function. Because the initial conditions are not in equilibrium with the applied static load the resulting displacement field is time dependent. However, if only consider e.g. the spatial interval $\hat{x} \in [-1,1]$ then the displacements become independent of time for $\hat{t} \geq 2$. In general we have ${}^L_T\hat{u}(\hat{x},\hat{t}\to\infty) = 0\,\forall\hat{x}$, while ${}^L_S\hat{u}(\hat{x})$ is the static solution for equations (1, 2, 52). This is illustrated in the following graphic

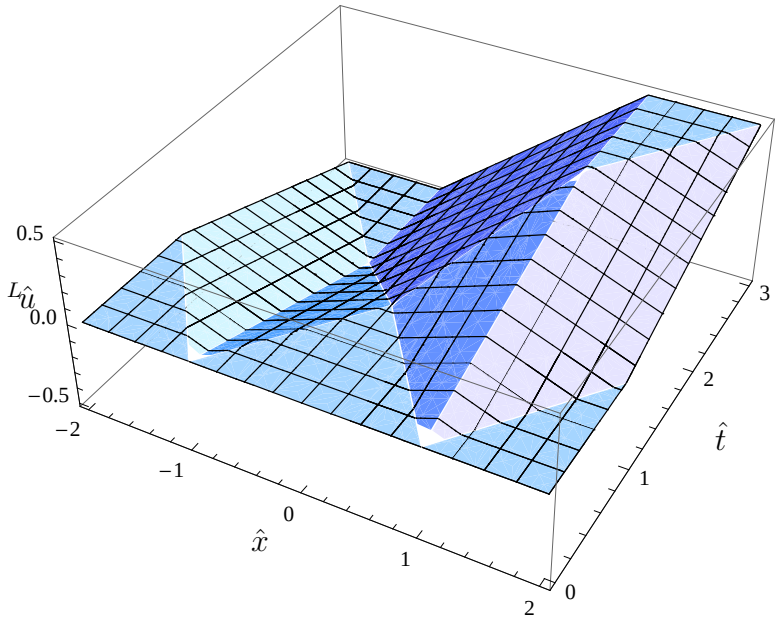

Fig. 3: Local solution $^{L}\hat{u}(\hat{x},\hat{t})$

4.1.2 Peridynamic non-local solution

Consider the following peridynamic material, characterized by the micromodulus function:

$$c(x;\delta) = \frac{E}{\delta^3}\frac{2}{\pi}\frac{\sin(x/\delta) - (x/\delta)\cos(x/\delta)}{(x/\delta)^3} \quad \Leftrightarrow \quad \omega(k;\delta) = \frac{c_0}{\delta}\begin{cases} k\delta & k\delta \leq 1 \\ 1 & k\delta > 1 \end{cases} \tag{57}$$

In the following we normalize the *material* length-scale associated with the non-local material model, the horizon δ, with the *geometrical* length-scale of the bar, L: $\hat{\delta} = \delta/L$.
The static solution defined in (1, 3, 52) can be found analytically using FOURIER transformations, $^{NL}_{S}\bar{u}(k;\delta) = \mathcal{F}_{1D}\{^{NL}_{S}u(x;\delta)\} \equiv \int_{-\infty}^{+\infty} e^{-ikx}u(x;\delta)dx$:

$$^{NL}_{S}\bar{u}(k;\delta) = \frac{\bar{b}(k)}{\bar{c}(0;\delta) - \bar{c}(k;\delta)} \tag{58}$$

$$\bar{b}(k) = -2\imath\frac{F}{A}\sin(kL) \tag{59}$$

$$\bar{c}(k;\delta) = \frac{E}{\delta^2}\frac{1-(k\delta)^2}{2}[\,\mathrm{sgn}(1-k\delta) + \mathrm{sgn}(1+k\delta)\,] \tag{60}$$

Returning to normalized variables we can solve the integrals required for the inverse transformation analytically by identifying the inverse of the 1D DIRAC distribution $\bar{\delta}(k) = 1$:

$$\begin{aligned} {}^{NL}_{S}\hat{u}(\hat{x};\hat{\delta}) &= \frac{1}{4}\left(\frac{2}{\pi}\,\mathrm{Si}(\frac{1+\hat{x}}{\hat{\delta}})(1+\hat{x}) - \frac{2}{\pi}\,\mathrm{Si}(\frac{1-\hat{x}}{\hat{\delta}})(1-\hat{x})\right) - \frac{\hat{\delta}}{\pi}\sin(\frac{1}{\hat{\delta}})\sin(\frac{\hat{x}}{\hat{\delta}}) \quad (61)\\ &\quad +\hat{\delta}^2[\,\frac{\Delta(\hat{x}-1)-\Delta(\hat{x}+1)}{2} + \frac{\cos(\frac{1}{\hat{\delta}})\sin(\frac{\hat{x}}{\hat{\delta}}) - \hat{x}\cos(\frac{\hat{x}}{\hat{\delta}})\sin(\frac{1}{\hat{\delta}})}{\pi(1-\hat{x}^2)}] \end{aligned}$$

with the integral sine function $\mathrm{Si}(z) = \int_0^z \frac{sin(t)}{t}dt$.
In the following we verify this solution numerically. We know that the solution is antisymmetric and we restrict out attention to $\hat{x} > 0$. Assuming a constant far field $\hat{u}(\hat{x}) = \hat{u}_\infty$ for $\hat{x} > \hat{x}_\infty \in \mathbb{N}$ we approximate the remaining integral over $[0, \hat{x}_\infty]$ in (3) by the composite midpoint rule to obtain the following equilibrium equations for the discrete displacements ${}^{NL}_{S}\hat{u}_i(\hat{\delta}) \approx {}^{NL}_{S}\hat{u}(\hat{x}_i;\hat{\delta})$, $\hat{x}_i = i/N$, $i = 1,\ldots,\hat{x}_\infty N - 1$:

$$\begin{aligned} {}^{NL}_{S}\underset{\sim}{\hat{u}}\,(\hat{\delta}) &= \underset{\sim}{\hat{c}}^{\,-1}\,\underset{\sim}{\hat{b}} \quad (62)\\ {}^{NL}_{S}\underset{\sim}{\hat{u}} &= ({}^{NL}_{S}\hat{u}_i)^T,\ \underset{\sim}{\hat{c}} = (\hat{c}_{i,j}),\ \underset{\sim}{\hat{b}} = (\hat{b}_i)^T\\ \hat{c}_{i,j} &= f(-\infty)\,\delta_{i,j} - \frac{\hat{c}(\hat{x}_j-\hat{x}_i) - \hat{c}(\hat{x}_j+\hat{x}_i)}{N}\\ \hat{b}_i &= \hat{b}(\hat{x}_i) + \hat{u}_\infty\left(\frac{\hat{c}(\hat{x}_\infty-\hat{x}_i) - \hat{c}(\hat{x}_\infty+\hat{x}_i)}{2N} + f(\hat{x}_\infty-\hat{x}_i) - f(\hat{x}_\infty+\hat{x}_i)\right) \text{ with}\\ f(\hat{z}) &= \int_{\hat{z}}^{\infty}\hat{c}(\hat{\xi})d\hat{\xi} \end{aligned}$$

For the material (57) we have

$$f(\hat{z}) = \hat{\delta}^{-2}[\,\frac{\sin(\psi)-\psi\cos(\psi)}{\pi\psi^2} + \frac{1}{2} - \frac{\mathrm{Si}(\psi)}{\pi}]_{\psi=\frac{\hat{z}}{\hat{\delta}}} \quad (63)$$

while the point load is represented by $\hat{b}(\hat{x}_i) = \frac{N\delta_{i,N}}{2}$.
In the following graphic we plot the analytical solution (61, blue line) as well as the linear interpolation of the numerical solution (62, dots connected by black line) together with the local solution (56, red dashed line) for $\hat{\delta} = 0.5$, $N = 10$, $\hat{x}_\infty = 2$, $u_\infty = 0.5$[10].

[10] In [10] it is shown that this is indeed the exact local as well as non-local far-field solution.

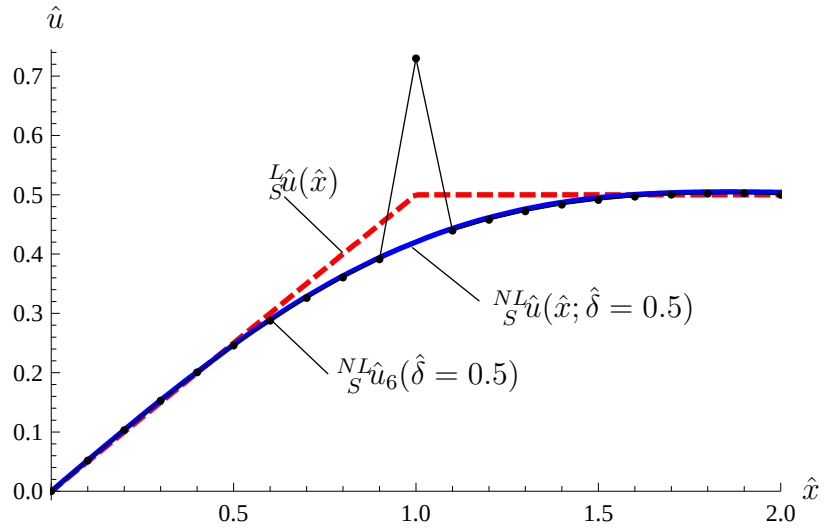

Fig. 4: Comparison of analytical and numerical solution for the static non-local case

We can see that already for this relatively coarse discretization with only 19 degrees of freedom the numerical values agree very well with the analytical values inside the loaded region $\hat{x} < 1$. At the location of the point load $\hat{x} = 1$ the discrete solution approximates the DIRAC distribution also predicted by the analytical solution. However, despite this singular loading the adjacent numerical displacements remain smooth. Finally at $\hat{x} = \hat{x}_\infty = 2$ we see a small jump caused by guessing the far-field displacements. Note that for large $\hat{x}_\infty \to \infty$ the choice of $\hat{u}_\infty$ becomes irrelevant for the solution (62) inside the region $\hat{x} < 1$.
Returning to the dynamic problem we find

$$
\begin{aligned}
{}^{NL}\hat{u}(\hat{x},\hat{t};\hat{\delta}) &= {}^{NL}_{T}\hat{u}(\hat{x},\hat{t};\hat{\delta}) + {}^{NL}_{S}\hat{u}(\hat{x};\hat{\delta}) \text{ with} && (64)\\
{}^{NL}_{T}\hat{u}(\hat{x},\hat{t};\hat{\delta}) &= \frac{1}{8}\,[\,\frac{2}{\pi}\,\mathrm{Si}(\frac{1-\hat{x}+\hat{t}}{\hat{\delta}})(1-\hat{x}+\hat{t}) + \frac{2}{\pi}\,\mathrm{Si}(\frac{1-\hat{x}-\hat{t}}{\hat{\delta}})(1-\hat{x}-\hat{t}) && (65)\\
&\quad -\frac{2}{\pi}\,\mathrm{Si}(\frac{1+\hat{x}+\hat{t}}{\hat{\delta}})(1+\hat{x}+\hat{t}) - \frac{2}{\pi}\,\mathrm{Si}(\frac{1+\hat{x}-\hat{t}}{\hat{\delta}})(1+\hat{x}-\hat{t})\,]\\
&\quad -\cos(\hat{t}/\hat{\delta})\,[\,\hat{\delta}^2\,\frac{\Delta(1-\hat{x})-\Delta(1+\hat{x})}{2}\\
&\qquad +\hat{\delta}^2\,\frac{\sin(\frac{\hat{x}}{\hat{\delta}})\cos(\frac{1}{\hat{\delta}})-\hat{x}\cos(\frac{\hat{x}}{\hat{\delta}})\sin(\frac{1}{\hat{\delta}})}{\pi\,(1-\hat{x}^2)} - \hat{\delta}\,\frac{\sin(\frac{1}{\hat{\delta}})\sin(\frac{\hat{x}}{\hat{\delta}})}{\pi}\,]
\end{aligned}
$$

Note that unlike in the local theory the "transient" response does not vanish for large $\hat{t}$. Instead we have undamped oscillations with the normalized angular frequency $1/\hat{\delta}$ and amplitude ${}^{NL}_{A}\hat{u}(\hat{x};\hat{\delta})$ around the static solution ${}^{NL}_{S}\hat{u}(\hat{x};\hat{\delta})$.

$$
\begin{aligned}
{}^{NL}_{LT}\hat{u}(\hat{x},\hat{t};\hat{\delta}) &= {}^{NL}_{T}\hat{u}(\hat{x},\hat{t}>>0;\hat{\delta}) = {}^{NL}_{S}\hat{u}(\hat{x};\hat{\delta}) + {}^{NL}_{A}\hat{u}(\hat{x};\hat{\delta})\,\cos(\hat{t}/\hat{\delta}) && (66)\\
{}^{NL}_{A}\hat{u}(\hat{x};\hat{\delta}) &= \hat{\delta}^2\,[\,\frac{\Delta(\hat{x}-1)-\Delta(\hat{x}+1)}{2} + \frac{\cos(\frac{1}{\hat{\delta}})\sin(\frac{\hat{x}}{\hat{\delta}})-\hat{x}\cos(\frac{\hat{x}}{\hat{\delta}})\sin(\frac{1}{\hat{\delta}})}{\pi(1-\hat{x}^2)}\,]
\end{aligned}
$$

4.1.3 Comparison of classical and Peridynamic solution

As pointed out in [41] the presence of a DIRAC distribution in the external loads leads to a DIRAC distribution in the displacement field under the point load in the non-local formulation. This is not the case in the local formulation. In this sense the local formulation seems more smooth. However, for all other points the opposite is true: while the strain field has a jump discontinuity in local elasticity it remains continuous in peridynamics, as illustrated in the following graphics

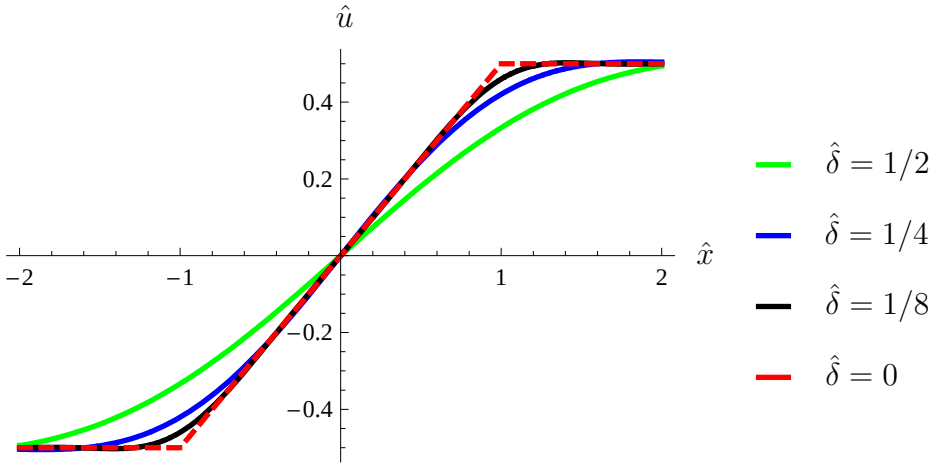

Fig. 5: Static solution in local elasticity and peridynamics

In the local formulation a static point load eventually (i.e. for $\hat{t} \to \infty$) leads to a static deformation field, see (56). This is not true in peridynamics where in the long time (LT) limit any point continuous to oscillate around the static solution ${}^{NL}_{S}\hat{u}(\hat{x};\hat{\delta})$ with frequency $1/\hat{\delta}$ and amplitude ${}^{NL}_{A}\hat{u}(\hat{x};\hat{\delta})$ as shown in (66). In the limit as $\hat{\delta} \to 0$ the frequency of these oscillations becomes infinite while the amplitude goes to zero: ${}^{NL}_{A}\hat{u}(\hat{x};\hat{\delta}) = O(\hat{\delta}^2)$. At the same time the static non-local solution converges to the static local solution (56), ${}^{NL}_{S}\hat{u}(\hat{x};\hat{\delta} \to 0) = {}^{L}\hat{u}(\hat{x})$. In the following graphics the local displacement under the point load ${}^{L}\hat{u}(\hat{x}=1,\hat{t})$ (red) is plotted together with the static non-local solution, ${}^{NL}_{S}\hat{u}(\hat{x}=1;\hat{\delta}=1/4)$ (black, solid), the dynamic non-local solution ${}^{NL}\hat{u}(\hat{x}=1,\hat{t};\hat{\delta}=1/4)$ (blue) as well as the amplitude of the predicted oscillations (black, dashed):

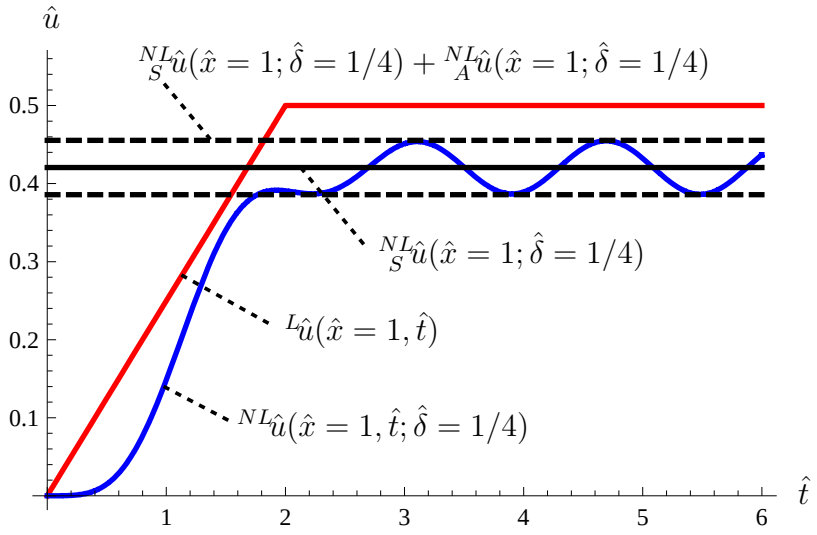

Fig. 6: Displacement $\hat{u}(\hat{x}=1,\hat{t})$ under the point load in local and non-local elasticity

According to (4, 52) the displacement under the point load can also be interpreted as the total energy of the system: $E_{tot}(t)=\frac{2F}{A}\,u(x=L,t)$. In local elasticity the total energy becomes constant for $\hat{t}\geq 2$ and the system is conservative. In peridynamics the point under the point load never comes to rest so the point forces continue to change the total energy.

4.2 Initial value problem for initial data with FOURIER-series representation (3D)

As an example consider the following initial displacement[11]

$$\boldsymbol{u}(\boldsymbol{x},0) \;=\; \boldsymbol{U}_0\cos(\boldsymbol{k}_0\cdot\boldsymbol{x}) \leftrightarrow \bar{\boldsymbol{u}}^0(\boldsymbol{k})=(2\pi)^3\boldsymbol{U}_0\frac{\Delta(\boldsymbol{k}+\boldsymbol{k_0})+\Delta(\boldsymbol{k}-\boldsymbol{k_0})}{2} \tag{67}$$

Then the solution follows from equation (49):

$$\bar{\boldsymbol{u}}(\boldsymbol{k},t) \;=\; \dot{\bar{\boldsymbol{g}}}(\boldsymbol{k},t)\cdot\left((2\pi)^3\boldsymbol{U}_0\frac{\Delta(\boldsymbol{k}+\boldsymbol{k_0})+\Delta(\boldsymbol{k}-\boldsymbol{k_0})}{2}\right) \tag{68}$$

$$\begin{aligned}\boldsymbol{u}(\boldsymbol{x},t) \;&=\; \dot{\bar{\boldsymbol{g}}}(\boldsymbol{k}_0,t)\cos(\boldsymbol{k}_0\cdot\boldsymbol{x})\cdot\boldsymbol{U}_0 \\ &=\; \left(\cos(\omega_{\parallel}(k_0)t)\,\boldsymbol{n}_{\boldsymbol{k}_0}\boldsymbol{n}_{\boldsymbol{k}_0}+\cos(\omega_{\perp}(k_0)t)\,\boldsymbol{P}_{\boldsymbol{n}_{\boldsymbol{k}_0}}\right)\cdot\boldsymbol{U}_0\cos(\boldsymbol{k}_0\cdot\boldsymbol{x})\end{aligned} \tag{69}$$

While the spatial distribution is identical in local and non-local elasticity the temporal dependence is generally different due to the nonlinear dispersion relation.

[11] Adding additional initial velocity is straight forward. Also this methodology can be easily extended to initial data with countably many wavenumbers, i.e. with FOURIER-series representation.

4.3 Static solution for a single point load (3D

The non-local static solution of (20)

$$\bar{\boldsymbol{u}}(\boldsymbol{k}) \;=\; \boldsymbol{M}^{-1}(\boldsymbol{k}) \cdot \bar{\boldsymbol{b}}(\boldsymbol{k}) \tag{70}$$

subjected to a point load at the origin, $\boldsymbol{b}(\boldsymbol{x}) = \boldsymbol{P}\delta(\boldsymbol{x})$, is given by

$$\begin{aligned}
\boldsymbol{u}(\boldsymbol{x}) &= \mathcal{F}^{-1}\{\boldsymbol{M}^{-1}(\boldsymbol{k})\} \cdot \boldsymbol{P} \quad \text{with} && (71)\\
\mathcal{F}^{-1}\{\boldsymbol{M}^{-1}(\boldsymbol{k})\} &= f_{\boldsymbol{n_x}}(x)\boldsymbol{n_x}\boldsymbol{n_x} + f_{\boldsymbol{P_{n_x}}}(x)\boldsymbol{P}_{\boldsymbol{n}_x} && (72)\\
f_{\boldsymbol{n_x}}(x) &= \frac{1}{2\pi^2}\int_0^\infty [\, a_1(xk)\left(\frac{k^2}{M_\perp(k)} - \frac{k^2}{M_\parallel(k)}\right) + \frac{\sin(kx)}{kx}\frac{k^2}{M_\perp(k)}\,]\, dk\\
f_{\boldsymbol{P_{n_x}}}(x) &= \frac{1}{2\pi^2}\int_0^\infty [\, a_2(xk)\left(\frac{k^2}{M_\perp(k)} - \frac{k^2}{M_\parallel(k)}\right) + \frac{\sin(kx)}{kx}\frac{k^2}{M_\perp(k)}\,]\, dk
\end{aligned}$$

where $x = ||\boldsymbol{x}||$. Substituting the component of the local acoustic tensor equation (22, 23) we obtain the well-known result, see e.g. [13]

$$^{L}\boldsymbol{u}(\boldsymbol{x}) \;=\; \frac{1}{8\pi\mu x}\left(2\,\boldsymbol{n_x}\boldsymbol{n_x} + \frac{\lambda+3\mu}{\lambda+2\mu}\boldsymbol{P}_{\boldsymbol{n_x}}\right)\cdot\boldsymbol{P} \tag{73}$$

In the non-local case the integrals given in eqs. (72) do not converge: the last term in the integrands is unbounded for large k since, unlike in the local case, the acoustic tensor is constant in this limit: $^{NL}M_\parallel(k), {}^{NL}M_\perp(k) \to {}^{NL}M^\infty$. The reason for this divergence is the presence of a DIRAC-distribution in the solution. When rewriting eqs. (72) to exclude the DIRAC-distribution, the remaining integrals converge:

$$\begin{aligned}
^{NL}f_{\boldsymbol{n_x}}(x) &= \frac{1}{2\pi^2}\int_0^\infty [\, a_1(xk)\left(\frac{k^2}{M_\perp(k)} - \frac{k^2}{M_\parallel(k)}\right) + \frac{\sin(kx)}{kx}\left(\frac{k^2}{M_\perp(k)} - \frac{k^2}{^{NL}M^\infty}\right)\,]\, dk\\
&\quad + \frac{\Delta(\boldsymbol{x})}{^{NL}M^\infty} && (74)\\
^{NL}f_{\boldsymbol{P_{n_x}}}(x) &= \frac{1}{2\pi^2}\int_0^\infty [\, a_2(xk)\left(\frac{k^2}{M_\perp(k)} - \frac{k^2}{M_\parallel(k)}\right) + \frac{\sin(kx)}{kx}\left(\frac{k^2}{M_\perp(k)} - \frac{k^2}{^{NL}M^\infty}\right)\,]\, dk\\
&\quad + \frac{\Delta(\boldsymbol{x})}{^{NL}M^\infty} && (75)
\end{aligned}$$

As an example we consider the exponential micromodulus function discussed in section 3.2.5. The results of the numerical integration is presented in the plots below for different degrees of non-locality $\delta > 0$, together with the local solution $\delta = 0$ with $\lambda = \mu$. On the left, the normalized displacement component $\frac{^{NL}f_{\boldsymbol{n_x}}(x)}{\mu}$ in the direction of $\boldsymbol{x}$ is shown while on the right the normalized displacement component $\frac{^{NL}f_{\boldsymbol{P_{n_x}}}(x)}{\mu}$ orthogonal to $\boldsymbol{x}$ is shown.

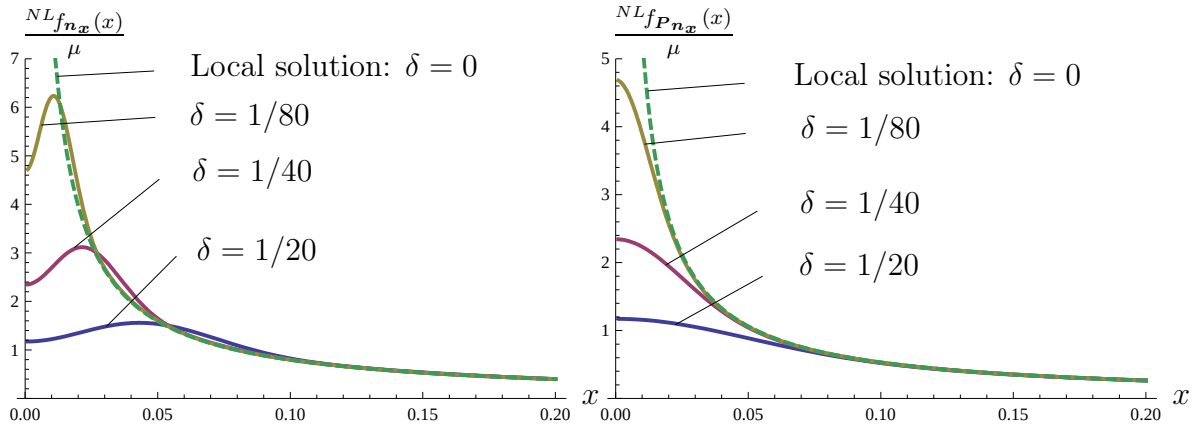

Fig. 7: Local and non-local deformation under a static point load

This numerical study indicates that in the limit of vanishing horizon $\delta \to 0$ the non-local solution converges towards the local solution almost everywhere. However, for any finite horizon $\delta > 0$ the displacements under the point load remain bounded[12] when ignoring the DIRAC-distribution[13].

In contrast the displacements in local elasticity are unbounded due to the presence of the $1/x$ singularity in the solution.

5 Conclusions

This paper concentrates on the comparison between the classical, local and the peridynamic, non-local formulation of linear elasticity. First we develop an integral representation for the solution of the 3D bond-based peridynamic equation of motion. Then we apply this theoretical result to a series of static and dynamic problems in 1D and 3D. We found that when subjecting a peridynamic material to a point load represented mathematically by a DIRAC distribution, the response will also include a DIRAC distribution. The presence of DIRAC distributions in the deformation field / GREEN's function is not unphysical since any physical loading function is always applied over a finite spatial domain. Applying the same point loading to the classical local material does not lead to a DIRAC response which suggest that in some sense the local response is smoother. However, that is not the complete picture. When disregarding DIRAC contributions, the remaining non-local deformations are actually in some sense more smooth: in 1D the strain field across a point load has a jump discontinuity within the local formulation but remains continuous in peridynamics. In 3D the local displacements have a $1/x$-type singularity when approaching the point load while the non-local displacements remain finite. This is perhaps not surprising

[12] In [24] the analogous result is obtained for the static GREEN's function within the context of the so-called quasicontinuum model of a perfect lattice of identical particles.

[13] If we had applied the external force field to a finite region in space the DIRAC-distribution would not be present in the solution.

as the motivation in some of the earlier work on weakly non-local methods was to remove the presence of the unphysical $1/x$-type singularities in the stress field surrounding a crack tip.
There are several interesting and challenging directions for future research in non-local elasticity:

- More complex / realistic external forces such as time-dependent point loads (either at a fixed spatial position, or moving in space), or spatially distributed loading.
- Non-local deformation and stress field surrounding a crack tip.
- More complex non-local material models, e.g. for anisotropic CFRP composites.
- Non-local boundary conditions and their relationship to the local boundary conditions (Dirichlet, Neumann, Robin).

Studying these problems would provide important theoretical insight and increase the fidelity of peridynamic simulations.

6 Acknowledgements

We would like to thank Prof. Florin Bobaru for a fruitful discussion at the ASME conference in Boston, Dr. Rich Lehoucq, Dipl.-Math. Dipl.-Ing. Juliane Dunkel for a careful and constructive critical reading, Dr. Michael Bieterman for initial finanical support and Dr. Greg Shubin for loaning us his copy of [4].
Sandia is a multiprogram laboratory operated by Sandia Corporation, a Lockheed Martin Company, for the United States Department of Energy's National Nuclear Security Administration under contract DE-AC04-94AL85000.

7 Appendix

7.1 Nomenclature

$\boldsymbol{v}$	Vector
v	Vector norm $v = \|\|\boldsymbol{v}\|\| = \sqrt{\boldsymbol{v} \cdot \boldsymbol{v}}$
$\boldsymbol{n_v}$	Normal vector $\boldsymbol{n_v} = \frac{\boldsymbol{v}}{v}$ $(v \neq 0)$
$\boldsymbol{ab}$	Dyadic product
$\boldsymbol{a} \cdot \boldsymbol{b}$	Dot product
$\boldsymbol{a} \times \boldsymbol{b}$	Cross product
$\boldsymbol{T}$	Tensor
$\boldsymbol{I}$	Identity tensor $\boldsymbol{T} \cdot \boldsymbol{I} = \boldsymbol{I} \cdot \boldsymbol{T} = \boldsymbol{T}$
$\boldsymbol{P}_n$	Projector $\boldsymbol{P}_n = (\boldsymbol{I} - \boldsymbol{nn})$
$\mathrm{Tr}(\cdot)$	Trace $\mathrm{Tr}(\boldsymbol{T}) = \boldsymbol{T} : \boldsymbol{I}$

δ_{ij}	Kronecker Delta $\delta_{ij} = \delta^{ij} = \begin{cases} 1 & i = j \\ 0 & i \neq j \end{cases}$
$\boldsymbol{e}_i = \boldsymbol{e}^i$	Cartesian basis $\boldsymbol{e}_i \cdot \boldsymbol{e}_j = \boldsymbol{e}^i \cdot \boldsymbol{e}^j = \delta_{ij}$
$\boldsymbol{x}$	Position vector $\boldsymbol{x} = \sum_{i=1}^{3} x_i \boldsymbol{e}_i$
$\nabla(\cdot)$	Gradient operator $\nabla(\cdot) = \sum_{i=1}^{3} \boldsymbol{e}_i \frac{\partial(\cdot)}{\partial x_i}$
t	Time
$\dot{\boldsymbol{f}}(\boldsymbol{x}, t)$	Time derivative $\dot{\boldsymbol{f}}(\boldsymbol{x}, t) = \frac{\partial \boldsymbol{f}(\boldsymbol{x}, t)}{\partial t}$
$\imath$	Imaginary unit $\imath^2 = -1$
$\Delta(x)$ / $\Delta(\boldsymbol{x})$	1D / 3D DIRAC distribution

7.2 FOURIERtransforms

7.2.1 Definition

In the cartesian basis $\{\boldsymbol{e}_i\}$ the FOURIERtransform $\bar{\boldsymbol{f}}(\boldsymbol{k})$ of the vector-valued function $\boldsymbol{f}(\boldsymbol{x}) = \sum_{i=1}^{3} f_i(x_j)\boldsymbol{e_i}$ of the three independent variables $x_j = \boldsymbol{e_j} \cdot \boldsymbol{x}$, $j = 1, 2, 3$ is defined as

$$\bar{\boldsymbol{f}}(\boldsymbol{k}) \equiv \mathcal{F}\{\boldsymbol{f}(\boldsymbol{x})\} := \int_{\mathbb{R}^3} e^{-i\boldsymbol{k}\cdot\boldsymbol{x}} \boldsymbol{f}(\boldsymbol{x}) dV_x \tag{76}$$

$$\boldsymbol{f}(\boldsymbol{x}) \equiv \mathcal{F}^{-1}\{\bar{\boldsymbol{f}}(\boldsymbol{k})\} = \frac{1}{(2\pi)^3} \int_{\mathbb{R}^3} e^{i\boldsymbol{k}\cdot\boldsymbol{x}} \bar{\boldsymbol{f}}(\boldsymbol{k}) dV_k \tag{77}$$

or in component form

$$\bar{f}_i(k_1, k_2, k_3) \equiv \mathcal{F}\{f_i(x_1, x_2, x_3)\} := \int_{\mathbb{R}^3} e^{-i(k_1 x_1 + k_2 x_2 + k_3 x_3)} f_i(x_1, x_2, x_3) dx_1 dx_2 dx_3$$

$$f_i(x_1, x_2, x_3) \equiv \mathcal{F}^{-1}\{\bar{f}_i(k_1, k_2, k_3)\} := \frac{1}{(2\pi)^3} \int_{\mathbb{R}^3} e^{i(k_1 x_1 + k_2 x_2 + k_3 x_3)} \bar{f}_i(k_1, k_2, k_3) dk_1 dk_2 dk_3$$

7.2.2 FOURIERtransforms of derivatives

The FOURIERtransform of the gradient of a tensor $\boldsymbol{T}$ is given by

$$\mathcal{F}\{\nabla \otimes \boldsymbol{T}\} = -i\boldsymbol{k} \otimes \mathcal{F}\{\boldsymbol{T}\} \tag{78}$$

where $\otimes \in \{\cdot, \, , \times\}$ is the dot product, dyadic product or the cross product. As an example the FOURIERtransform of the derivative of a scalar function $f(x, y, z)$ with respect to x is given by $\mathcal{F}\{\partial_x f(x, y, z)\} \equiv \mathcal{F}\{\boldsymbol{e}_x \cdot \nabla f\} = -i\boldsymbol{e}_x \cdot \boldsymbol{k}\bar{f}(k_x, k_y, k_z) = -ik_x \bar{f}(k_x, k_y, k_z)$.

7.2.3 Convolution theorem

The convolution of the two function $\boldsymbol{f}(\boldsymbol{x})$ and $\boldsymbol{g}(\boldsymbol{x})$ is defined as follows

$$\boldsymbol{h}(\boldsymbol{x}) := \int_{\mathbb{R}^3} \boldsymbol{f}(\hat{\boldsymbol{x}}) \otimes \boldsymbol{g}(\boldsymbol{x} - \hat{\boldsymbol{x}}) dV_{\hat{x}} = \int_{\mathbb{R}^3} \boldsymbol{f}(\boldsymbol{x} - \hat{\boldsymbol{x}}) \otimes \boldsymbol{g}(\hat{\boldsymbol{x}}) dV_{\hat{x}} \tag{79}$$

where $\otimes \in \{\cdot, , \times\}$ is the dot product, dyadic product or the cross product between the two vector-valued functions $\boldsymbol{f}$ and $\boldsymbol{g}$. Then the FOURIERtransform of $\boldsymbol{h}(\boldsymbol{x})$ is given by $\bar{\boldsymbol{h}}(\boldsymbol{k}) = \bar{\boldsymbol{f}}(\boldsymbol{k}) \otimes \bar{\boldsymbol{g}}(\boldsymbol{k})$.

7.3 LAPLACEtransforms

7.3.1 Definition

In cartesian basis $\{\boldsymbol{e}_i\}$ the LAPLACEtransform $\tilde{\boldsymbol{f}}(s)$ of the vector-valued function $\boldsymbol{f}(t)$ is defined as

$$\tilde{\boldsymbol{f}}(s) \equiv \mathcal{L}\{\boldsymbol{f}(t)\} := \int_0^\infty \exp(-st)\boldsymbol{f}(t)dt \tag{80}$$

$$\boldsymbol{f}(t) \equiv \mathcal{L}^{-1}\{\tilde{\boldsymbol{f}}(s)\} = \frac{1}{\imath}\int_{\gamma-\imath\infty}^{\gamma+\imath\infty} \exp(st)\tilde{\boldsymbol{f}}(s)ds \tag{81}$$

7.3.2 LAPLACEtransforms of derivatives

$$\mathcal{L}\{\boldsymbol{f}^{(n)}(t)\} = s^n\tilde{\boldsymbol{f}}(s) - \boldsymbol{f}(+0)s^{n-1} - \boldsymbol{f}'(+0)s^{n-2} - \ldots - \boldsymbol{f}^{(n-2)}(+0)s - \boldsymbol{f}^{(n-1)}(+0) \tag{82}$$

7.3.3 Convolution theorem

The convolution of the two function $\boldsymbol{f}(t)$ and $\boldsymbol{g}(t)$ is defined as follows

$$\boldsymbol{h}(t) := \int_0^t \boldsymbol{f}(\tau) \otimes \boldsymbol{g}(t-\tau)d\tau \tag{83}$$

where $\otimes \in \{\cdot, , \times\}$ is the dot product, dyadic product or the cross product between the two vector-valued functions $\boldsymbol{f}$ and $\boldsymbol{g}$. Then the LAPLACEtransform of $\boldsymbol{h}(\boldsymbol{x})$ is given by $\tilde{\boldsymbol{h}}(s) = \tilde{\boldsymbol{f}}(s) \otimes \tilde{\boldsymbol{g}}(s)$.

References

[1] 44th AIAA Aerospace Sciences Meeting and Exhibit. *Peridynamic Analysis of Damage and Failure in Composites*, volume 88, Reno, Nevada, January 2006. E. Askari and J. Xu and S. A. Silling.

[2] 48th AIAA Structures, Structural Dynamics, and Materials Conference. *Damage and Failure Analysis based on Peridynamics - Theory and Applications*. O. Weckner and A. Askari and J. Xu and H. Razi and S. A. Silling, 2007.

[3] 48th AIAA Structures, Structural Dynamics, and Materials Conference. *Damage and Failure Analysis Failure Analysis of Composite Laminates under Biaxial Loads*. J. Xu and A. Askari and O. Weckner and H. Razi and S. A. Silling, 2007.

[4] K. Aki and P. G. Richards. *Quantitative Seismology*. University Science Books, 2002.
[5] B. S. Altan. Uniqueness of initial-boundary value problems in nonlocal elasticity. *Int. J. Solids Structures*, 25(11), 1989.
[6] B. S. Altan. Uniqueness in nonlocal thermoelasticity. *J. Thermal Stresses*, 14, 1991.
[7] K. J. Bathe, editor. *Dynamic fracture modeling with a meshfree peridynamic code*. Computational Fluid and Solid Mechanics, S. A. Silling, 2003.
[8] Z. P. Bažant and M. Jirásek. Nonlocal integral formulations of plasticity and damage: survey and progress. *J. Eng. Mech.*, 128(11):1119–1149, 2002.
[9] F. Bobaru. Influence of van der waals forces on increasing the strength and toughness in dynamic fracture of nanofiber networks: a peridynamic approach. *Modeling and Simulation in Materials Science and Engineering*, 15:397–417, 2007.
[10] F. Bobaru, M. Yang, L. F. Alves, S. A. Silling, E. Askari, and J. Xu. Convergence, adaptive refinement, and scaling in 1d peridynamics. *International Journal for Numerical Methods in Engineering*, 77:852–877, 2009.
[11] Y. Chen, J. D. Lee, and A. Eskandarian. Atomistic viewpoint of the applicability of microcontinuum theories. *Int. J. Solids Structures*, 41(8):2085–2097, 2004.
[12] K. Dayal and K. Bhattacharya. Kinetics of phase transformations in the peridynamic formulation of continuum mechanics. *J. Mech. Phys. Solids*, 54:1811–1842, 2006.
[13] G. Eason, J. Fulton, and I. N. Sneddon. The generation of waves in an infinite elastic solid by variable body forces. *Mathematical and Physical Sciences Series A*, 995(248):575–607, 1956.
[14] W. C. Elmore and M. A. Heald. *Physics of Waves*. Dover Publications.
[15] E. Emmrich and O. Weckner. Analysis and numerical approximation of an integro-differential equation modelling non-local effects in linear elasticity. *Mathematics and Mechanics of Solids*, 12(4):363–384, 2005.
[16] E. Emmrich and O. Weckner. On the well-posedness of the linear peridynamic model and its convergence towards the navier equation of linear elasticity. *Communications in Mathematical Sciences*, 5(4):851–864, 2007.
[17] A. C. Eringen. Linear theory of nonlocal elasticity and dispersion of plane waves. *Int. J. Eng. Science*, 10:425–435, 1972.
[18] A. C. Eringen. Vistas of nonlocal continuum physics. *Int. J. Eng. Sci.*, 30(10):1551–1565, 1992.
[19] A.C. Eringen and D.G.B. Edelen. On nonlocal elasticity. *Int. J. Engng. Sci.*, 1972:232–248, 10.
[20] L. Li *et al.*, editor. *Peridynamic modeling of concrete structures*, Ia-FRAMCOS. W. Gerstle and N. Sau, 2004.
[21] L. Li *et al.*, editor. *Peridynamic modeling of plain and reinforced concrete structures*, SMiRT18. Int. Conf. Struct. Mech. React. Technol., W. Gerstle and N. Sau and S. A. Silling, 2005.
[22] K. F. Graff. *Wave Motion in Elastic Solids*. Dover Publ., 1991.
[23] E. Kröner. Elasticity theory of materials with long range forces. *Int. J. Solids Structures*, 3:731–742, 1967.

[24] I. A. Kunin. *Elastic Media with Microstructure I and II*. Springer, 1983.
[25] R. B. Lehoucq and S. A. Silling. Force flux and the peridynamic stress tensor. *Journal of the Mechanics and Physics of Solids*, 56:1566–1577, 2008.
[26] Y. Lei, M. I. Friswell, and S. Adhikari. A galerkin method for distributed systems with non-local damping. *Int. J. Solids Structures*, DOI 10.1016/j.ijsolstr.2005.06.058, 2005.
[27] Materials and Design: Numiform 2004. *Peridynamic 3D problems of nanofiber networks and carbon nanotube-reinforced composites*. F. Bobaru and S. A. Silling, 2004.
[28] R. S. Mindlin. Second gradient of strain and surface-tension in linear elasticity. *Int. J. Solids and Structures*, 1:417–438, 1965.
[29] F. J. Moody, editor. *Peridynamic modeling of impact damage*. American Society of Mechanical Engineers PVP-Vol. 489, S. A. Silling, E. Askari, 2004.
[30] M. L. Parks, R. B. Lehoucq, S. J. Plimpton, and S. A. Silling. Implementing peridynamics within a molecular dynamics code. *Computer Physics Communications*, 179:777–783, 2008.
[31] A. A. Pisano and P. Fuschi. Closed form solution for a nonlocal elastic bar in tension. *Int. J. Solids Structures*, 40(1):13–23, 2003.
[32] C. Polizzotto. Nonlocal elasticity and related variational principles. *Int. J. Solids Structures*, 38:42–43, 2001.
[33] D. Rogula. *Nonlocal Theory of Material Media*. Springer, 1982.
[34] SAMPE Fall Technical Conference. *The Design of a Hybrid Material for Multifunctional Performance using Advanced Analysis Techniques and Testing*. S. A. Silling and A. Askari and K. Nelson and O. Weckner and J. Xu., 2008.
[35] S. A. Silling. Emu. http://www.sandia.gov/emu/emu.htm.
[36] S. A. Silling. Reformulation of elasticity theory for discontinuities and long-range forces. *J. Mech. Phys. Solids*, 48(1):175–209, 2000.
[37] S. A. Silling and E. Askari. A meshfree method based on the peridynamic model of solid mechanics. *Computers & Structures*, 83(17-18):1526–1535, 2005.
[38] S. A. Silling and F. Bobaru. Peridynamic modeling of membranes and fibers. *Int. J. Non-linear Mech.*, 40(2-3):395–409, 2005.
[39] S. A. Silling, M. Epton, O. Weckner, J. Xu, and E. Askari. Peridynamics states and constitutive modeling. *Journal of Elasticity*, 88(2):151–184, 2007.
[40] S. A. Silling and R. B. Lehoucq. Convergence of peridynamics to classical elasticity theory. *Journal of Elasticity*, DOI 10.1007/s10659-008-916-3.
[41] S. A. Silling, M. Zimmermann, and R. Abeyaratne. Deformation of a peridynamic bar. *J. Elasticity*, 73:173–190, 2003.
[42] A. C. Eringen. *Continuum Physics II: Continuum Mechanics of Single-Substance Bodies*. Academic Press, 1975.
[43] J. Wang and R. S. Dhaliwal. On some theorems in the nonlocal theory of micropolar elasticity. *Int. J. Solids Structures*, 30(10):1331–1338, 1993.
[44] J. Wang and R. S. Dhaliwal. Uniqueness in generalized nonlocal thermoelasticity. *J. Thermal Stresses*, 16:71–77, 1993.
[45] T. Warren, S. A. Silling, A. Askari, O. Weckner, M. Epton, and J. Xu. A non-ordinary

state-based peridynamic method to model solid material deformation and fracture. *International Journal of Solids and Structures*, DOI 10.1016/j.ijsolstr.2008.10.029.

[46] O. Weckner and R. Abeyaratne. The effect of long-range forces on the dynamics of a bar. *J. Mech. Phys. Solids*, 53(3):705–728, 2005.

[47] O. Weckner and E. Emmrich. The peridynamic equation and its spatial discretisation. *Journal of Mathematical Modelling and Analysis*, 12(1):17–27, 2007.

[48] XI Int. Conf. Fract. *Peridynamic fracture and damage modeling of membranes and nanofiber networks*. F. Bobaru and S. A. Silling and H. Jiang, 2005.

[49] J. Xu, A. Askari, O. Weckner, and S. A. Silling. Peridynamic analysis of impact damage in composite laminates. *Journal of Aerospace Engineering*, 21(3):187–194, 2008.